A Polarization-/Angle-Insensitive, Bandwidth-Optimized, Metamaterial Absorber in the Microwave Regime

Alexandros I. Dimitriadis, Nikolaos V. Kantartzis, and Theodoros D. Tsiboukis

Department of Electrical and Computer Engineering,
Aristotle University of Thessaloniki, Thessaloniki GR-54124, Greece
*corresponding author, E-mail: aldimitr@auth.gr

Abstract

An enhanced metamaterial absorber based on the circumscribed-cross resonator is introduced in this paper. The new structure is polarization-independent, due to the symmetry of its unit cell, and is proven efficient for the attenuation of obliquely incident waves. The absorption mechanism is thoroughly investigated and is found to be mainly related to the losses of the dielectric substrate. Furthermore, by exploiting the scalability property of metamaterials, the operational bandwidth of our design can be drastically improved by placing unit cells with properly scaled resonators adjacent to each other. In this context, various combinations of three, four, and nine unit cells, that can increase the full width at half maximum up to as much as 11.18%, are developed. The overall performance of the proposed configurations is deemed promising for the realization of microwave metamaterial absorbers for several practical applications.

1. Introduction

Metamaterial absorbers have, recently, triggered a notable scientific investigation with an escalating impact on modern microwave systems. To this objective, the combination of an electric-LC (ELC) resonator with a split-wire has been proposed for the construction of an almost perfect arrangement, which, in its initial design, has been very sub-wavelength (around $\lambda_0/35$) [1]. Although quite narrowband and basically effective only for normally incident waves, this device inspired several researchers to probe its absorption mechanism [2], [3]. In the meanwhile, a considerable variety of instructive ideas have been launched in order to produce efficient metamaterial absorbers in the microwave, terahertz, and infrared frequency regions [4]-[10].

However, contemporary real-world applications, like RCS minimization from airplanes, steamboats and other vehicles or protection from electromagnetic interference due to mobile phones and local area networks, require more sophisticated features, while preserving the ultra-thin size of the original approach. Amid them, one can discern the larger bandwidth or multiple bands of operation as well as the wide-angle and polarization-independent absorption rates [11]-[17]. Essentially, most of the structures reported in the literature focus on the improvement of just one of the prior characteristics, thus turning the construction of an overall optimized device into a challenging design problem.

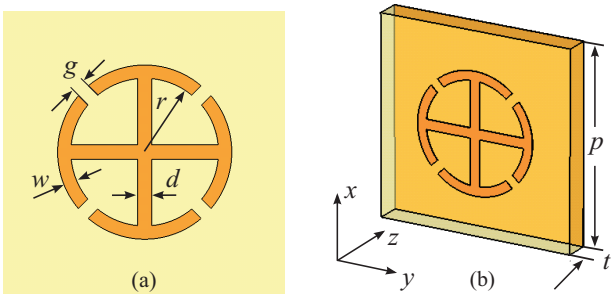

Figure 1: (a) Front and (b) perspective view of the CCR absorber. Dimensions: $r = 2.06\,\text{mm}$, $d = 0.40\,\text{mm}$, $g = 0.39\,\text{mm}$, $w = 0.37\,\text{mm}$, $p = 8\,\text{mm}$, and $t = 1\,\text{mm}$.

In this paper, a novel metamaterial absorber with improved bandwidth performance that operates around the middle of the microwave X-band ($8.0 - 12.0\,\text{GHz}$), is presented. The proposed design, implemented by means of the circumscribed-cross resonator (CCR), exhibits remarkable wide-angle absorption and independence on the polarization of the incident radiation. Moreover, taking avail of metamaterial scalability, the operational bandwidth of the structure is significantly enhanced by combining appropriately tailored unit cells in certain periodic arrangements. In this way, the demanding obliquely incident waves are efficiently absorbed, without any other non-physical conventions. The merits of the optimized absorber are thoroughly validated via different metal and dielectric material setups, while some possible future extensions are finally discussed.

2. Theory and design of the CCR absorber

The primary design concept of the proposed device is based on the CCR, depicted in Fig. 1a, which belongs to the class of ELC resonators [18] and its first resonance is usually excited by an electric field component parallel to one of its crossed wires. The CCR is imprinted on a standard 1 mm-thick FR-4 substrate ($\varepsilon_r = 4.3$, $\tan\delta = 0.022$), whereas the opposite face of the dielectric spacer is covered with a copper layer (Fig. 1b), so as to ensure zero transmission throughout the structure. Additionally, periodic boundary conditions are applied along the x- and y-axis in order to model an infinite array of unit cells. For our analysis, all simulations are carried out through the frequency domain solver of CST MWS$^{\text{TM}}$ computational package [19].

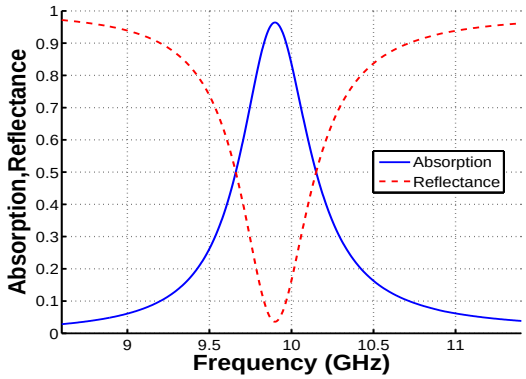

Figure 2: Absorption and reflectance of the proposed structure. The absorption peak of 96.41% occurs at the frequency of 9.90 GHz and the FWHM is 4.96%.

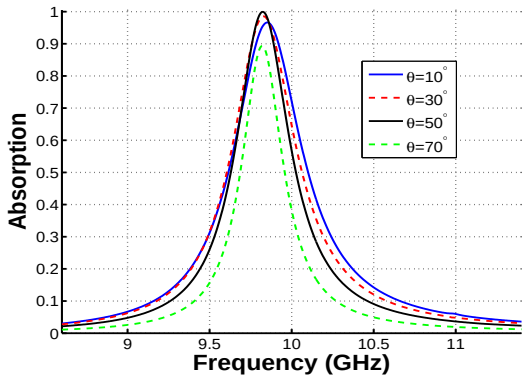

Figure 3: Absorption for various θ angles and $\phi = 0°$.

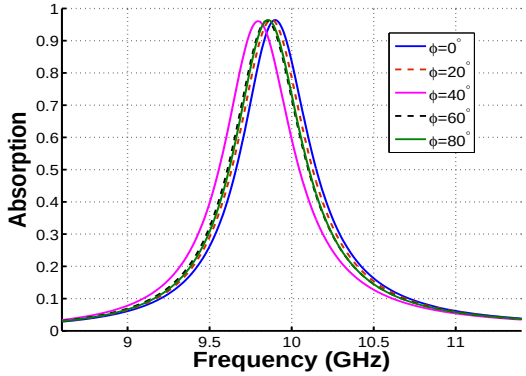

Figure 4: Absorption for various ϕ angles and $\theta = 0°$.

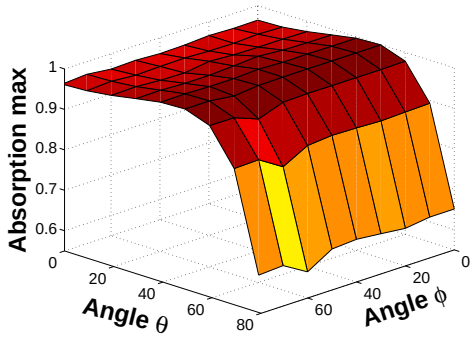

Figure 5: Absorption maximum for various combinations of obliquely incident waves (variations of θ and ϕ angles from $0°$ to $80°$, with a $10°$ increment for both of them).

Starting with arbitrary dimensions and considering a normally incident plane wave propagating along the z-direction with its electric-field component polarized along the x-axis, a genetic algorithm is employed to reach the optimal unit cell parameters for maximum absorption near the middle of the X-band. The absorption of the structure is calculated from the values of the simulated scattering parameters through its definition as $A(\omega) = 1 - R(\omega) - T(\omega)$, with $R(\omega) = |S_{11}|^2$ and $T(\omega) = |S_{21}|^2$ being the reflectance and transmittance, respectively. Since $T(\omega) = 0$ due to the copper plane, Fig. 2 illustrates the reflectance and absorption of the device, revealing an absorption peak of 96.41% at 9.90 GHz and a full width at half maximum (FWHM) of 4.96% around this center frequency. Note, also, that the complete symmetry of the unit cell along the x- and y-direction ensures the accomplishment of similar absorptive behavior for arbitrary polarizations of the incident wave.

3. Angle-independent absorption characteristics of the CCR absorber

In this section, the response of our device to obliquely incident radiation is examined. To this end, angles θ and ϕ are defined, as those formed between the propagation vector of the incident wave and the z-axis over the yz- and xz-plane, respectively (see Fig. 1b for axes definition). Initially, angle θ is varied, while keeping $\phi = 0°$. The corresponding absorption curves are illustrated in Fig 3, indicating an almost angle-independent performance up to $\theta = 70°$. On the other hand, by setting $\theta = 0°$ and varying angle ϕ, Fig 4 is obtained. Again, the absorption spectrum remains almost unchanged, except for a slight downshift of the maximum absorption frequency for $\phi = 40°$.

Although the above results constitute a strong indication for the angle-insensitive performance of the proposed absorber, it is crucial to explore the most general case of obliquely incident radiation. For this goal, angles θ and ϕ are varied simultaneously (with a step of $10°$ each). The peak absorption values for all possible angle combinations, are given in the surface plot of Fig. 5. Very efficient absorption for any angle ϕ and for θ values up to $70°$ can be promptly observed. However, slight variations in the center frequency of the maximum absorption occur, especially for angles larger than $60°$, as provided in Table 1. These findings are indeed very promising and seem to even transcend other similar results available in the literature [15].

4. Investigation of the loss mechanism

The absorption mechanism should be an issue of systematic investigation, since it can offer valuable physical interpretations. Actually, there are two generally accepted loss mechanisms; dielectric losses arising from the imaginary part of

Table 1: Maximum absorption frequency $f_{\max}$ (GHz) for various oblique incidence angles θ and ϕ.

Angle ϕ	Angle θ				
	$0°$	$20°$	$40°$	$60°$	$80°$
$0°$	9.90	9.84	9.81	9.83	9.80
$20°$	9.88	9.86	9.85	9.82	9.72
$40°$	9.80	9.79	9.76	9.61	9.67
$60°$	9.85	9.83	9.83	9.62	9.61
$80°$	9.85	9.88	9.85	9.83	9.71

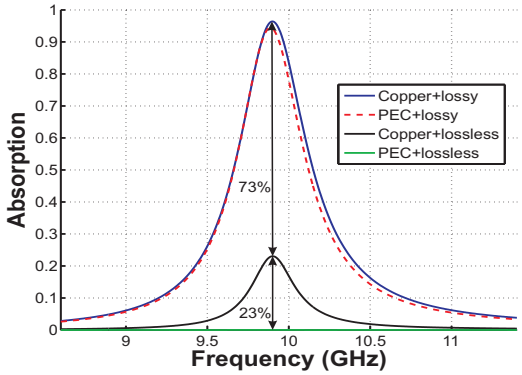

Figure 6: Absorption performance for different dielectrics (lossless or lossy) and metal properties (copper or PEC).

the substrate's dielectric constant and ohmic losses due to the finite conductivity of the structure's metallic parts.

Herein, we perform additional simulations for all possible combinations of dielectric (lossless or lossy) and metal (copper with finite conductivity or perfectly electric conductor (PEC)) types to reveal their actual contribution to the absorption performance, presented in Fig. 6. As expected, the PEC-lossless dielectric case exhibits zero absorbance over the whole frequency range. Moreover, in the copper-lossless substrate scenario, $A(\omega)$ reaches a peak value of 23% at 9.90 GHz. Such an outcome could lead to the assumption that both absorption mechanisms are involved in the CCR structure with additive effects. Nonetheless, in the case of a lossy dielectric, the absorbance plot remains almost unchanged when replacing copper with a PEC material, substantiating that practically only dielectric losses affect the optimized absorber's overall performance.

5. Bandwidth-enhanced variants

To further enhance the absorption bandwidth of the novel design, the scalability property of metamaterials is utilized. In particular, by multiplying the dimensions of the original CCR along the x- and y-axis with a scaling factor s, the center frequency can be downshifted ($s > 1$) or upshifted ($s < 1$), while the absorption curve retains its original shape and fractional bandwidth. This property may be used for the synthesis of multiband absorbers, as in [15]. It is mentioned that unit cells with different absorbing frequencies, owing to their scaled CCRs, can be alternately placed to form a multiband absorbing metasurface.

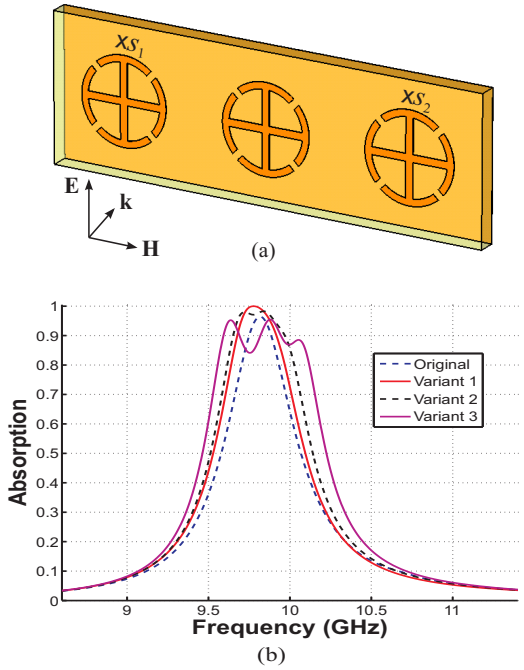

Figure 7: (a) Combined structure with three unit cells and (b) absorption performance of variants with different scaling factors, as explained in Table 2.

Table 2: Scaling factors and FWHM for the different variants of Fig. 7b.

	Orig.	Var. 1	Var. 2	Var. 3
s_1	1.000	0.990	0.985	0.980
s_2	1.000	1.010	1.015	1.020
FWHM	4.96%	5.66%	6.36%	7.68%

In this framework, we employ a similar idea to the original unit cell of Section 2, which can be considered as the borderline case of a multiband design. Specifically, by arranging unit cells with scaling factors very close to unity, adjacent to each other, a new, larger unit cell is formed with multiple overlapping absorptive regions. In the following subsections, diverse implementations with three, four, and nine unit cells are suggested and studied in order to improve the FWHM of the initially introduced CCR absorber.

5.1. Three unit-cells

First, our approach is applied to a set of three unit cells (Fig. 7a). As observed, two scaled unit cells, with scaling factors s_1 and s_2, respectively, are combined with the original one. Three different variants with enhanced FWHM values are illustrated in Fig. 7b, for the scaling factors summarized in Table 2. It becomes apparent that for scaling factors gradually departing from unity, the absorption spectrum of each individual unit cell starts to discriminate from the whole, leading to decreased overlapping and lower absorption peaks. However, it is stressed that in all variants of Fig. 7b, the FWHM is significantly increased from 4.96% of the original unit cell up to 7.68% for variant 3.

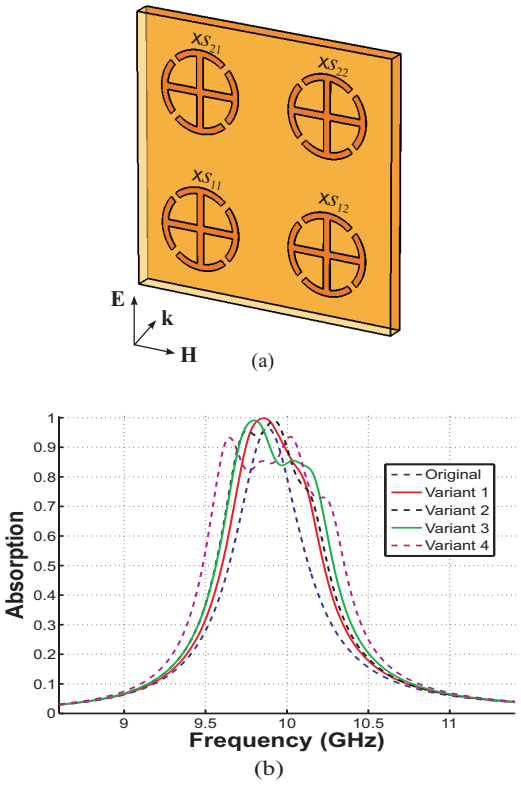

Figure 8: (a) Combined structure with four unit cells and (b) absorption performance of variants with different scaling factors, as explained in Table 3.

Table 3: Scaling factors and FWHM for the different variants of Fig. 8b.

	Orig.	Var. 1	Var. 2	Var. 3	Var. 4
s_{11}	1.000	0.985	1.000	0.980	0.970
s_{12}	1.000	1.005	0.980	1.010	0.990
s_{21}	1.000	1.015	1.020	1.020	1.010
s_{22}	1.000	0.995	1.000	0.990	1.030
FWHM	4.96%	6.36%	6.97%	7.37%	8.79%

5.2. Four unit-cells

Next, the same concept is utilized in a set of four unit cells, as in Fig. 8a. Various possibilities arise by properly controlling scaling factors s_{ij}, for $(i, j) = 1, 2$. Specifically, four different variants with improved FWHM values are demonstrated in Fig. 8b, for the scaling factors listed in Table 3. Again, we can readily detect the considerable bandwidth enhancement that is achieved through the pertinent selection of s_{ij}. For instance, in variant 4 of Fig. 8b, the FWHM is increased from 4.96% of the original unit cell to 8.79%.

5.3. Nine unit-cells

As our final configuration, we investigate the combined device of Fig. 9a, comprising nine unit cells, which offers additional design perspectives via the appropriate choice of scaling factors s_{ij}, for $(i, j) = 1, 2, 3$. In a similar fashion with the scenario of the previous subsection, four different variants with enhanced values of FWHM are considered and their performance is shown in Fig. 9b, for the scaling factors of Table 4. From the results, one can deduce that in all variants the FWHM is significantly raised; from 4.96% of the original unit cell up to 11.18% for variant 4.

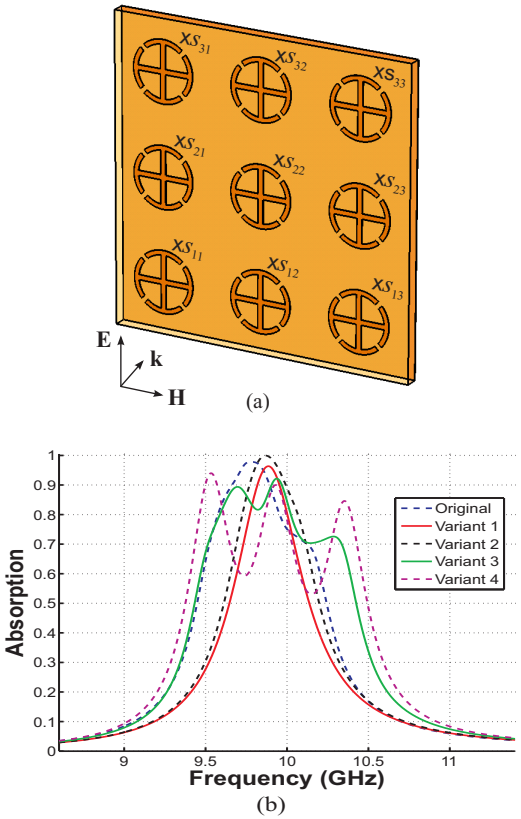

Figure 9: (a) Combined structure with nine unit cells and (b) absorption performance of variants with different scaling factors, as explained in Table 4.

Table 4: Scaling factors and FWHM for the different variants of Fig. 9b.

	Orig.	Var. 1	Var. 2	Var. 3	Var. 4
s_{11}	1.000	1.000	1.000	1.000	1.000
s_{12}	1.000	0.985	0.980	0.980	0.960
s_{13}	1.000	1.005	1.010	1.020	1.040
s_{21}	1.000	1.010	1.015	1.020	1.040
s_{22}	1.000	1.000	1.000	1.000	1.000
s_{23}	1.000	0.990	0.985	0.980	0.960
s_{31}	1.000	0.995	0.990	0.980	0.960
s_{32}	1.000	1.015	1.020	1.020	1.040
s_{33}	1.000	1.000	1.000	1.000	1.000
FWHM	4.96%	5.98%	8.08%	9.96%	11.18%

6. Discussion and conclusions

A class of robust metamaterial absorbers based on the CCR geometry has been presented in this paper. The proposed devices have been shown to exhibit several attractive characteristics, such as wide-angle and polarization-insensitive

absorption, by implementing an electrically thin ($\lambda_0/30$ at the resonance frequency), low-cost FR-4 dielectric substrate. In essence, analysis has proven that their performance is principally related to the dielectric losses of the substrate. Additionally, the possibility to attain bandwidth-enhanced structures has been extensively discussed and the FWHM of the original unit cell has been increased from 4.96% to 11.18%. Possible extensions of the new absorber can be envisaged in terms of tunable metamaterials, as an alternative path to performance-enhanced components. For example, by loading the CCRs with varactor elements, a fully controllable surface may be attained, as in [20], providing supplementary degrees of freedom to the design procedure presented herein. Hence, the aforementioned assets can render this structure a potential candidate for diverse real-world applications in the microwave spectrum.

Acknowledgement

This research has been co-financed by the EU (European Social Fund − ESF) and Greek national funds through the Operational Program "Education and Lifelong Learning" of the National Strategic Reference Framework (NSRF) − Research Funding Program: Heracleitus II. Investing in knowledge society through the European Social Fund.

References

[1] F.M. Landy, S. Sajuyigbe, J.J. Mock, D.R. Smith, W.J. Padilla, Perfect metamaterial absorber, *Phys. Rev. Lett.* 100: pp. 207402(1–3), 2008.

[2] C.G. Hu, X. Li, Q. Feng, X.N. Chen, X.G. Luo, Investigation on the role of the dielectric loss in metamaterial absorber, *Opt. Express* 18: pp. 6598–6603, 2010.

[3] T. Wang, L. Wang, Y. Nie, R. Gong, Relation between dielectric spacer thickness and absorption feature in metamaterials absorber, *Proc. Int. Symp. Sign. Syst. and Electron.*, Nanjing, China, pp. 1–4, 2010.

[4] H. Tao, C.M. Bingham, A.C. Strikwerda, D. Pilon, D. Shrekenhamer, N.I. Landy, K. Fan, X. Zhang, W.J. Padilla, R.D. Averitt, Highly flexible wide angle of incidence terahertz metamaterial absorber: Design, fabrication and characterization, *Phys. Rev. B* 78: pp. 241103R(1–4), 2008.

[5] Q.Y. Wen, H.W. Zhang, Y.S. Xie, Q.H. Yang, Y.L. Liu, Dual band terahertz metamaterial absorber: Design, fabrication, and characterization, *Appl. Phys. Lett.* 95: pp. 241111(1–3), 2009.

[6] Y. Avitzour, Y.A. Urzhumov, G. Shvets, Wide-angle infrared absorber based on a negative-index plasmonic metamaterial, *Phys. Rev. B* 79: pp. 045131(1–5), 2009.

[7] F. Bilotti, A. Toscano, K.B. Alici, E. Ozbay Hu, L. Vegni, Design of miniaturized narrowband absorbers based on resonant-magnetic inclusions, *IEEE Trans. Electomagn. Compat.* 53: pp. 63–72, 2011.

[8] J. Sun, L. Liu, G. Dong, J. Zhou, An extremely broad band metamaterial absorber based on destructive interference, *Opt. Express* 19: pp. 21155–21162, 2011.

[9] W. Zhu, X. Zhao, B. Gong, L. Liu, B. Su, Optical metamaterial absorber based on leaf-shaped cells, *Appl. Phys. A - Mater.* 102: pp. 147–151, 2011.

[10] M. Pu, Q. Feng, M. Wang, C. Hu, C. Huang, X. Ma, Z. Zhao, C. Wang, X. Luo, Ultrathin broadband nearly perfect absorber with symmetrical coherent illumination, *Opt. Express* 20: pp. 2246–2254, 2012.

[11] J. Lee, S. Lim, Bandwidth-enhanced and polarisation-insensitive metamaterial absorber using double resonance, *Electron. Lett.* 47: pp. 8–9, 2011.

[12] Y. Cheng, H. Yang, Z. Cheng, N. Wu, Perfect metamaterial absorber based on a split-ring-cross resonator, *Appl. Phys. A - Mater.* 102: pp. 99–103, 2011.

[13] H. Li, L.H. Yuan, B. Zhou, X.P. Shen, Q. Cheng, T.J. Cui, Ultrathin multiband gigahertz metamaterial absorbers, *J. Appl. Phys.* 110: pp. 014909(1–8), 2011.

[14] L.K. Sun, H.F. Cheng, Y.J. Zhou, J. Wang, Low-frequency and broad band metamaterial absorber: Design, fabrication, and characterization, *Appl. Phys. A - Mater.* 105: pp. 49–53, 2011.

[15] L. Li, Y. Yang, C. Liang, A wide-angle polarization-insensitive ultra-thin metamaterial absorber with three resonant modes, *J. Appl. Phys.* 110: pp. 063702(1–5), 2011.

[16] Q. Ye, Y. Liu, H. Lin, M. Li, H. Yang, Multi-band metamaterial absorber made of multi-gap SRRs structure, *Appl. Phys. A - Mater.*, pp. 1–6, 2012.

[17] Y.Z. Cheng, Y. Wang, Y. Nie, R.Z. Gong, X. Xiong, X. Wang, Design, fabrication and measurement of a broadband polarization-insensitive metamaterial absorber based on lumped elements, *J. Appl. Phys.* 111: pp. 044902(1–4), 2012.

[18] H.T. Chen, J.F. O'Hara, A.J. Taylor, R.D. Averitt, C. Highstrete, M. Lee, W.J. Padilla, Complementary planar terahertz metamaterials, *Opt. Express* 11: pp. 1127–1130, 2011.

[19] Computer Simulation Technology, *CST MWS™: Computer Simulation Technology: Microwave Studio*, 2011.

[20] W. Withayachumnankul, C. Fumeaux, D. Abbott, Planar array of electric-LC resonators with broadband tunability, *IEEE Antennas Wireless Propag. Lett.* 10: pp. 577–580, 2011.